Queen's University Belfast

Structure of warm dense matter via angularly resolved x-ray scatter

Riley, D., Angulo Gareta, J., Garcia Saiz, M., Khattak, F., Kohanoff, J., Sahoo, S., ... Neely, D. (2009). Structure of warm dense matter via angularly resolved x-ray scatter. Plasma Physics and Controlled Fusion, 51(12), [124036]. DOI: 10.1088/0741-3335/51/12/124036

Published in:
Plasma Physics and Controlled Fusion

Document Version:
Publisher's PDF, also known as Version of record

Queen's University Belfast - Research Portal:
Link to publication record in Queen's University Belfast Research Portal

Publisher rights
© 2009 IOP Publishing

General rights
Copyright for the publications made accessible via the Queen's University Belfast Research Portal is retained by the author(s) and / or other copyright owners and it is a condition of accessing these publications that users recognise and abide by the legal requirements associated with these rights.

Take down policy
The Research Portal is Queen's institutional repository that provides access to Queen's research output. Every effort has been made to ensure that content in the Research Portal does not infringe any person's rights, or applicable UK laws. If you discover content in the Research Portal that you believe breaches copyright or violates any law, please contact openaccess@qub.ac.uk.

Download date:15. Feb. 2017

IOPscience

HOME | SEARCH | PACS & MSC | JOURNALS | ABOUT | CONTACT US

Structure of warm dense matter via angularly resolved x-ray scatter

This article has been downloaded from IOPscience. Please scroll down to see the full text article.

2009 Plasma Phys. Control. Fusion 51 124036

(http://iopscience.iop.org/0741-3335/51/12/124036)

The Table of Contents and more related content is available

Download details:
IP Address: 143.117.23.73
The article was downloaded on 20/11/2009 at 16:01

Please note that terms and conditions apply.

Plasma Phys. Control. Fusion **51** (2009) 124036 (6pp) doi:10.1088/0741-3335/51/12/124036

Structure of warm dense matter via angularly resolved x-ray scatter

D Riley[1], J J Angulo Gareta[1], E García Saiz[1], F Y Khattak[1], J Kohanoff[1], S Sahoo[1], G Shabbir Naz[1], S F C Shearer[1], K A Thornton[1], C Gregory[2], N C Woolsey[2], M Notley[3] and D Neely[3]

[1] School of Mathematics and Physics, Queens University Belfast, Belfast BT7 1NN, UK
[2] Department of Physics, University of York, Heslington, York YO10 5DD, UK
[3] Central Laser Facility, Rutherford Appleton-Laboratory OX11 OQX, UK

E-mail: d.riley@qub.ac.uk

Received 19 June 2009, in final form 10 September 2009
Published 11 November 2009
Online at stacks.iop.org/PPCF/51/124036

Abstract
In this paper we describe experimental results on angularly resolved x-ray scatter from a sample of warm dense aluminium that has been created by double sided laser-driven shock compression. The experiment was carried out on the Central Laser Facility of the Rutherford Appleton Laboratory, using the VULCAN laser. The form of the angularly resolved scatter cross-section was compared with predictions based on a series of molecular dynamics simulations with an embedded atom potential, a Yukakwa potential and a bare Coulomb potential. The importance of screening is evident from the comparison and the embedded atom model seems to match experiment better than the Yukawa potential.

(Some figures in this article are in colour only in the electronic version)

1. Introduction

Warm dense matter (WDM) is a state of matter that is of significant scientific interest. It is a state intermediate between the solid state, where Coulomb forces dominate over thermal motion and classical plasmas where the converse is the case. Its physical characteristics include partial electron degeneracy with $T \sim T_F$ where T_F is the Fermi temperature and strong ion–ion coupling; quantified by the *strong coupling parameter*:

$$\Gamma = \frac{(Ze)^2}{ak_B T_i}, \tag{1}$$

where a is the ion-sphere radius, T_i is the ion temperature and Z is the average ionization. This parameter is important in determining the microscopic arrangement of the ions, which at values of $\Gamma \geqslant 10$ starts to resemble that of a liquid metal [1]. Such matter is of importance,

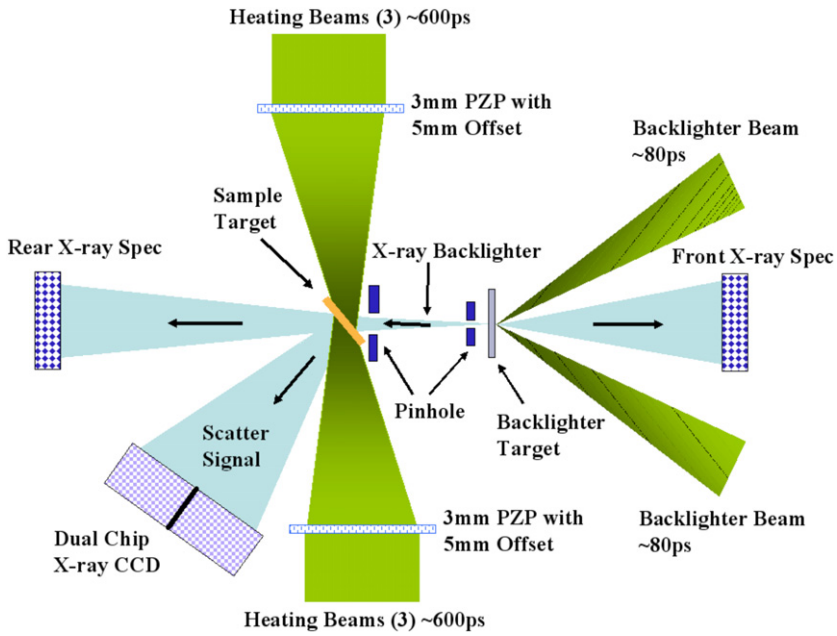

Figure 1. Schematic of the experiment.

primarily due to its relevance to planetary interiors [2] and inertial fusion experiments. One method for diagnosing such matter is by x-ray scattering [3–5]. For a quasi-monochromatic x-ray scatter source we can expect a spectrally integrated scatter signal, $I(q)$, of the form below [6, 7];

$$I(q) = I_{\mathrm{T}}\left[(f_{\mathrm{i}}(q) + \rho(q))^2 S_{\mathrm{ii}}(q) + Z_{\mathrm{b}} S^{\mathrm{inc}}(q) + Z_{\mathrm{f}} S_{\mathrm{ee}}(q)\right], \tag{2}$$

where q is the scatter momentum, $I_{\mathrm{T}}(q)$ is the classical Thomson cross-section for an electron, $f_{\mathrm{i}}(q)$ is the ionic form factor, $\rho(q)$ is the electron–ion correlation term and $S_{\mathrm{ii}}(q)$ is the static ion–ion structure factor. These terms come together to give us the quasi-coherent Rayleigh scatter from the ions. The terms $S^{\mathrm{inc}}(q)$ and $S_{\mathrm{ee}}(q)$ refer, respectively, to the incoherent bound-free Compton scatter from Z_{b} bound electrons and the static electron structure factor for scatter from Z_{f} free electrons per atom. For a moderate Z plasma at modest temperature, the latter two terms are usually small compared with the Rayleigh scatter, e.g. for Al at the range of conditions in the current experiment, the Thomas Fermi model leads us to expect between 10 and 11 bound electrons on average compared with two or three free electrons. Since the ionic form factor factor scales as Z^2, we can see how Rayleigh scatter dominates. Indeed, in an earlier paper [8] it was seen in high resolution scatter spectra that the Rayleigh scatter was clearly dominant over incoherent (spectrally shifted) scatter.

2. Experimental arrangements

The experiment was performed at the Rutherford Appleton Laboratory using the multi-beam laser facility VULCAN. A schematic of the experiment is shown in figure 1. The main six beams, delivering nominally 600 ps pulses of 200 J each in IR, were frequency doubled to 527 nm (with up to 100 J per beam) and synchronously focused in two opposing groups of three onto the sample. The focusing optics made use of phased zone plates (PZPs) combined

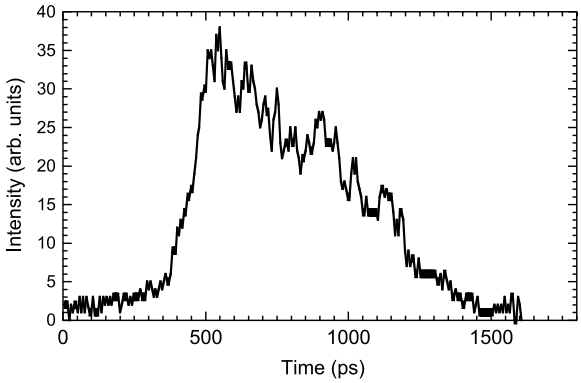

Figure 2. Optical streak measurement of the temporal profile for the shock driving pulse.

with $f/10$ lens to generate a 3 mm flat topped focal spot (with 5 mm offset from the best focus to reduce the level of the associated central spike). As can be seen from figure 1 the sample foil was at 45° to the incident beams, meaning that they created an elliptical focal spot with major and minor diameters of 4.2 mm and 3 mm, respectively. The pulse shape in second harmonic was measured with the use of an optical streak camera and can be seen in figure 2. The peak intensity achieved on target was $\sim 4.5 \times 10^{12}\,\mathrm{W\,cm^{-2}}$. By careful adjustment of beam energies, the balance between the opposing bunches was kept to within ~10%. The use of three beams per side was useful in keeping the shock drives balanced as it smoothed out shot to shot fluctuations on individual beams.

The target itself consisted of a CH/Al/CH sandwich with thicknesses 4.5/6/4.5 μm. In figure 3 we can see a HYADES [9] simulation of the density and temperature for three different times after the start of the pulse reaching the target surface. The slight asymmetry is a result of 10% imbalance in the beams for the shot and illustrates the maximum asymmetry typically encountered. The graphs show only the conditions for the Al core of the sample. The simulation used multi-group radiation transfer with 35 groups logarithmically spaced from 0.01–15 keV and the SESAME equation of state tables [10]. In an earlier publication [8] we showed that for one sided irradiation of similar targets at similar pulse durations and intensities, the time for shock breakout predicted by HYADES closely matched experimental measurements, the extent that we have enough confidence in the simulated plasma conditions to be confident of conclusions drawn from the experimental scatter data. Two shorter pulse beams of 80 ps duration were also frequency doubled and synchronously focused with $f/10$ lenses onto a 3 μm thick Ti target to generate the backlighting x-ray beam. The intensity on target was controlled by changing the focal spot dimension. The back-lighter x-ray signal principally consisted of the He-α line ($1s^2$–$1s2p\ ^1P$ and satellites) emission at 4.7–4.75 keV. This is by far the dominant spectral feature in the few kiloelectronvolts spectral region and for the intensities used here has a duration similar to the optical pulse [11] thus allowing ~100 ps resolution. The emission level was monitored with the help of two flat-crystal spectrometers coupled CCD systems, one in the rear employing Si (1 1 1) and one in the front of the target making use of Ge(2 2 0) crystal. After passing through an array of two pinholes, the probing x-ray back-lighter beam was restricted to a narrow cone which determines the angular resolution of the experiment. This narrow cone was then incident on the sample. However, high resolution restricts the incident signal to a lower signal level and a spread of 4° was employed as a compromise between resolution and signal level. This meant that the x-ray probe covered a

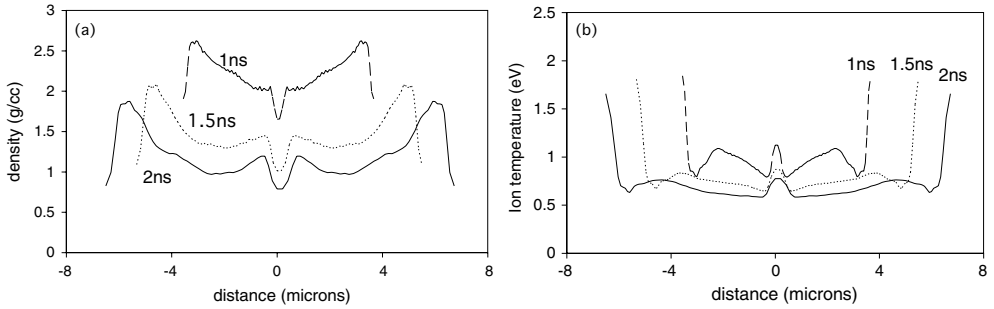

Figure 3. (*a*) Mass density profile for double sided illumination at 5 TW cm^{-2} at 1, 1.5 and 2 ns after the peak of the driving pulse. (*b*) Ion temperature for same conditions and timings

focal spot $\sim 1 \times 1.4$ mm, somewhat smaller than the shocked area. By delaying the back-lighter beams relative to the shock driving beams, the back-lighter x-rays could be made to probe the sample at a range of times relative to the shock compression. An Andor dual-chip x-ray CCD system, covering a range from 50° to 80° scattered angle, was used in the photon counting mode to detect the scattered signal. Appropriate shielding was in place to prevent x-rays from the back-lighter source from hitting the CCD directly. As for previous experiments, in order to ensure that we have only scattering from the shock compressed region, we took several test shots where the entire assembly including the target holder was put into place but without the actual sample foil—the subsequent shots resulted in detected photon counts less than 5% of the typical scatter signals, thus demonstrating that our signals come from the shocked sample.

The dual-chip CCD has two chips of 27.6×6.9 mm^2 dimension sited side by side. The chips were ∼12 cm from the sample. Each third of a chip thus subtended ∼4.5° thus matching the angular resolution of the probe cone of x-rays. We made histograms centred about five positions on each chip so as to 'over-sample'. Filtering of 250 μm Be, 72 μm Mylar and 39μm Al allowed transmission of just under 6% of the Ti-He-α photons whilst severely suppressing the kiloelectronvolt photon emission from the hot CH plasma on the surface of the samples. As in earlier, work, [12] we use single photon counting to measure the number of photons scattered into each unit of solid angle. Although the crystal spectrometers monitoring the throughput of the back-lighter source onto the target gave us shot to shot comparisons, the crystals were not absolutely calibrated and so comparisons with theory in this paper are made with respect to variation with angle rather than absolute cross-sections.

3. Experimental results

In figure 4 we can see cross-section measurements taken at 1.5 ns and at 2 ns after the start of the shock driving beams with conditions similar to those illustrated in figure 3. The error bars are based on counting statistics of the photons in each histogram. We have compared the data with some simulations. Firstly, we can see that the one component plasma (OCP) model, which assumes that the ions are embedded in a uniform electron gas and interact via the bare Coulomb potential, predicts a distinctive peak. However, a molecular dynamics model based on an embedded atom potential fits the shape of the experimental data very well. The embedded atom model [14] was developed from condensed matter physics but has been applied to liquid metals [15] and has been used to investigate phenomena such as melting and freezing [16]. This type of model effectively accounts for multi-body interactions and screening via a potential that includes direct pair potentials as well as the energy of embedding an atom in the local

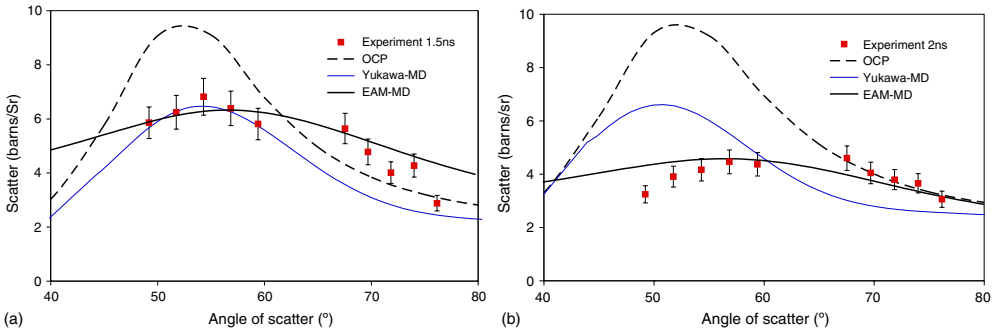

Figure 4. Scatter cross-section at two different delay times compared with three models. Note that, because we do not have an absolute calibration, the experimental data have been scaled to the level of the EAM–MD model. However, comparison of the shape of the cross-section as a function of angle leads to clear conclusions. The OCP model shows a distinctive peak, which is clearly reduced on introducing screening with a Yukawa type potential. However, it is clearly the embedded atom–MD model that fits quite well in both cases.

electron density contributed by all neighbours. Its parameters are generally adjusted to match experimental values for a range of thermodynamic properties. We have used this type of model previously [8, 16]. We do not have calibrations of the crystal spectra and CCD single pixel counting efficiencies, although estimates of these yield cross-sections within a factor of 2 of those expected. Accordingly, in the absence of accurate calibrations, we have scaled the experimental data to best show the fit to the EAM–MD model in this case. We can readily understand why the unscreened OCP does not work by considering the screening length, λ, expected for the electron gas to screen the ions (eg see [13]):

$$\lambda^{-2} = \frac{4e^2 m_\mathrm{e}}{\pi\hbar^3} \int f_e(p)\,\mathrm{d}p, \tag{3}$$

where $f_\mathrm{e}(p)$ is the Fermi–Dirac distribution for electrons with momentum, p. By using this, we can calculate that for the conditions of figure 3, we have $\lambda/a \sim 0.3$. We can note that, in equation (1), we define the strong coupling parameter in terms of a bare Coulomb interaction between the ions, yielding values of $\Gamma \sim 60$–80. If the interaction is screened with a screening length λ defined above, we can define an effective strong coupling parameter $\Gamma' = \Gamma \exp(-a/\lambda)$ and, with the screening calculated above, $\Gamma' \sim 2$–3. The electron–electron radius, r_s in units of the Bohr radius is ~2.7–3 for this data and the OCP is only expected to really apply when $r_s < 1$. With this in mind, we have also compared the data with a screened Coulombic potential of the form

$$V(r) = \frac{Ze^2}{4\pi\epsilon_0 r}\mathrm{e}^{-r/\lambda} \tag{4}$$

with λ determined as in equation (3). We can see that, although the effects of screening are obvious from comparison with the OCP, the fit to the data is still not as good as for the EAM–MD simulation. We note, in passing, that for the data, it appears that the peak in scatter is at a higher angle for the later time, lower density case. This is counter-intuitive and may be a result of the broadness of the peak which, combined with statistical uncertainty (the error bars represent only one standard deviation), serves to make the exact peak position less well defined.

4. Conclusions

We have made angularly resolved x-ray scatter measurements from a WDM sample. The electron density is not high enough to allow screening by electrons to be neglected. By using an embedded atom model we have fitted the shape of the data well, although we do not have absolute calibration. A comparison with an unscreened simulation shows the degree to which screening makes a difference. Interestingly, a model using a linear screening model (Yukawa potential) did not match the data as well as the embedded atom approach. In future experiments it may be possible to gather data from more uniform samples with smaller statistical error bars in order to make detailed investigations of the ion–ion structure factor and different approaches to its calculation.

Acknowledgment

This work was funded by the UK Engineering and Physical Sciences Research Council grants EP/D031532/1 and GR/R09572/01.

References

[1] Hansen J-P and McDonald I R 2006 *Theory of Simple Liquids* 3rd edn (New York: Academic)
[2] Ichimaru S 1982 *Rev. Mod. Phys.* **54** 1017
[3] Woolsey N C, Riley D and Nardi E 1998 *Rev. Sci. Instrum.* **69** 418
[4] Riley D *et al* 2000 *Phys. Rev. Lett.* **84** 1704
[5] Glenzer S H *et al* 2003 *Phys. Rev. Lett.* **90** 175002
[6] Chihara J 2000 *J. Phys.: Condens. Matter* **12** 231
[7] Nardi E 1991 *Phys. Rev.* A **43** 1977
[8] Garcia Saíz E 2008 *Phys. Rev. Lett.* **101** 075003
[9] Larsen J T and Lane S M 1994 *J. Quant. Spectrosc. Radiat. Transfer* **51** 179
[10] Lyon S P and Johnson J D 1992 *Group T-1, Los Alamos National Laboratory Technical Report LA-UR-92E3407*
[11] Riley D, Woolsey N C, McSherry D, Khattak F Y and Weaver 2002 *Plasma Sources Sci. Technol.* **11** 484
[12] Riley D, Woolsey N C, McSherry D and Nardi E 2000 *J. Quant. Spectrosc. Radiat. Transfer* **65** 463
[13] Wünsch K, Vorberger J and Gericke D O 2009 *Phys. Rev.* E **79** 010201 R
[14] Daw M S and Baskes M I 1984 *Phys. Rev.* B **29** 6443
[15] Mei J, Davenport J W and Fernando G W 1990 *Phys. Rev.* B **43** 4653
[16] Mei J and Davenport J W 1992 *Phys. Rev.* B **46** 21